Boundary-Layer Meteorol (2010) 135:109–132
DOI 10.1007/s10546-010-9466-3

ARTICLE

Comparison Between Large-Eddy Simulation and Reynolds-Averaged Navier–Stokes Computations for the MUST Field Experiment. Part I: Study of the Flow for an Incident Wind Directed Perpendicularly to the Front Array of Containers

J. L. Santiago · A. Dejoan · A. Martilli · F. Martin · A. Pinelli

Received: 22 December 2008 / Accepted: 21 January 2010 / Published online: 11 February 2010

Abstract The large-eddy simulation (LES) and Reynolds-averaged Navier–Stokes (RANS) methodologies are used to simulate the air flow inside the container's array geometry of the Mock Urban Setting Test (MUST) field experiment. Both tools are assessed and compared in a configuration for which the incident wind direction is perpendicular to the front array. The assessment is carried out against available wind-tunnel data. Effects of including small geometrical irregularities present in the experiments are analysed by considering LES and RANS calculations on two geometries: an idealized one with a perfect alignment and an identical shape of the containers, and a second one including the small irregularities considered in the experiment. These effects are assessed in terms of the local time-mean average and as well in terms of spatial average properties (relevant in atmospheric modelling) given for the velocity and turbulent fields. The structural flow properties obtained using LES and RANS are also compared. The inclusion of geometrical irregularities is found significant on the local time-mean flow properties, in particular the repeated flow patterns encountered in a perfect regular geometry is broken. LES and RANS provide close results for the local mean streamwise velocity profiles and shear-stress profiles, however the LES predictions are closer to the experimental values for the local vertical mean velocity. When considering the spatial average flow properties, the effects of geometrical irregularities are found insignificant and LES and RANS provide similar results.

Keywords Flow around array of obstacles · Large-eddy simulation · MUST experiment · Reynolds-averaged Navier–Stokes

J. L. Santiago (✉) · A. Martilli · F. Martin
Environment Department, Research Center for Energy, Environment and Technology (CIEMAT),
Av. Complutense 22, 28040 Madrid, Spain
e-mail: jl.santiago@ciemat.es

A. Dejoan · A. Pinelli
Energy Department, Research Center for Energy, Environment and Technology (CIEMAT),
Av. Complutense 22, 28040 Madrid, Spain

1 Introduction

Air quality is of growing concern in the urban environment and an accurate prediction of transport and dispersion of contaminants is needed. However, the complex surface morphology (buildings and other obstacles) that forms the urban canopy makes difficult the study of such a physical process. The interaction between the atmospheric turbulent boundary layer and the urban geometry generates complex flow patterns that determine the distribution of urban pollutant concentrations. Measurements of the dispersion of pollutants in urban areas or around obstacles have been carried out in several wind-tunnel or water-tunnel experiments (e.g., Meroney et al. 1996; Pavageau and Schatzmann 1999; Kastner-Klein and Plate 1999; Cheng and Castro 2002; Castro et al. 2006; Yee et al. 2006) and also in field experiments (e.g., Biltoft 2001; Dobre et al. 2005). Simple models such as Gaussian plume models, widely used in application for simple terrain, perform poorly for the prediction of urban environment dispersion because the complex geometry formed by bluff bodies such as buildings has to be explicitly modelled to correctly represent the interaction between the urban canopy and the atmospheric flow. Details of the flow around buildings can be tackled using the computational fluid dynamics (CFD) approach, which has been extensively used in simulations of dispersion phenomena in urban regions during this last decade. An "exact" numerical approach would rely upon the use of direct numerical simulation (DNS), where all the scales of the turbulence motion are resolved, thus allowing for obtaining very detailed information on the flow field. However, due to its computational cost, DNS is still restricted to the study of turbulent flow around an isolated building or around a limited number of obstacles (Yakhot et al. 2006; Coceal et al. 2006). On the other hand, the Reynolds-averaged Navier–Stokes (RANS) approach considers an integral approach for the whole turbulence spectrum so that turbulence modelling assumptions are required for the statistical closures. This approach does not require large computing resources and is the most commonly used. For example, Kim and Baik (2004), Santiago et al. (2007), and Milliez and Carissimo (2007) made use of RANS for the calculation of flow over idealized urban geometries, while Flaherty et al. (2007) and Michioka and Sato (2009) carried out RANS simulations over real urban geometries. An intermediate approach is the large-eddy simulation (LES) methodology, which, by means of a spatial filtering operation applied to the Navier–Stokes equations, resolves explicitly the dynamics of the unsteady large scales of turbulence while modelling the effect of small-scale motions on the resolved ones. Application of LES in the urban environment has been pursued by Hanna et al. (2002), Cheng et al. (2003), and Xie and Castro (2006) in flows over an array of regular cubes and by Camelli et al. (2005) and Tseng et al. (2006) and very recently by Michioka and Sato (2009) and Xie and Castro (2009) in field scale flows. Potentially, the capabilities of LES for the simulation of urban dispersion are superior to RANS; however, its applicability is more problematic due to the large computing time required (unsteady three-dimensional fields must be considered) compared to RANS and also to some issues regarding the implementation of wall and inlet conditions.

Comparative studies between RANS and LES approaches for flows over urban geometries are scarcely available. Cheng et al. (2003) compared the air flow computed by LES and RANS models over an array of cubes and found that both LES and RANS methodologies predicted reasonably well the main characteristics of the mean flow. They also stressed that, for their study, the LES computational cost was approximately 100 times greater than RANS. Xie and Castro (2006) showed that RANS and LES provide comparable results above the canopy layer of a flow over a staggered array of cubes, although the details of the field within the canopy were better captured by LES.

Even if CFD models can be applied successfully to simulate the flow over the complex morphology of a city, they present some limitations regarding their computational cost and can thus not be easily applied to air quality studies that include the whole city and its surroundings. In this case, numerical atmospheric models with simplified urban canopy models are most commonly used in order to catch the mesoscale features. In this context, the urban-obstacle effects within the canopy layer must be parameterised. Several parameterisations based on a horizontally-averaged approach have been recently proposed (Martilli et al. 2002; Coceal and Belcher 2004) for the modelling of the urban canopy. However, the validation of the parameterisation is still a difficult issue due to the lack of information on the spatially-averaged variables required for the parameterisation itself. In this context, CFD models can be a useful tool to provide flow variables with high enough spatial resolution to compute accurate values of the spatially-averaged properties over zones that are comparable to the grid-cell volume used in mesoscale models. Martilli and Santiago (2007) and Santiago et al. (2008) made use of the RANS approach for obtaining spatially-averaged flow properties in their parameterisation study of flow over an idealized urban geometry. The spatially-averaged flow properties were also extracted from DNS data by Coceal et al. (2006) for a simplified geometry.

A very interesting field experiment for urban environment dispersion simulation purposes is the Mock Urban Setting Test (MUST) experiment set up in the Great Desert (USA) to investigate the dispersion of a passive scalar within an array of containers (Biltoft 2001). This flow configuration was also studied in wind-tunnel and water-channel experiments (Yee et al. 2006; Leitl et al. 2007). Moreover, with its relatively simple geometry, it has also been extensively used for the evaluation of urban CFD models, using RANS (Milliez and Carissimo 2007; Di Sabatino et al. 2009) and, to a lesser extent, employing LES (Camelli et al. 2005).

In the present study we apply both LES and RANS methodologies to simulate the MUST experiment. Our study is divided into two parts. In this Part I we focus on the comparisons of the flow properties obtained with RANS and LES and propose the following:

(1) Establish a comparison methodology between RANS and LES performed in the limit of the grid resolution that ensures that the large building-scale flow is reasonably resolved. The minimum grid resolution required to obtain acceptable predictions using LES for the flow in an urban environment is not well established. The grid resolution used here lies between the requirements given by Tseng et al. (2006) and by Xie and Castro (2006). This kind of comparison is particularly significant for practical applications, if the difference in computing costs between the two modelling approaches is considered. The comparison between LES and RANS proposed here is based on two flow-scale levels: the local microscale (urban-street flow scales), relevant to the dispersion patterns within the urban canopy, and the mesoscale (extracted from the spatially-averaged flow properties), relevant to the development and validation of urban-layer parameterisation in atmospheric modelling.

(2) Establish the effects of small irregularities upon the flow within an array of urban-like obstacles. This is significant, for example, if we want to generalize results obtained for a specific configuration (idealized or real) to other similar but simplified configurations. Part of the numerical investigations that focus upon the MUST flow configuration does not include the small topological irregularities (different size of containers and not perfect alignment of the containers within the array) in the calculations (Yee et al. 2006; Milliez and Carissimo 2007) while others take them into account (Camelli et al. 2005; Di Sabatino et al. 2009). In general, the effects of their inclusion or omission on the

local microscale and on spatially-averaged flow properties were not discussed in these previous studies.

These issues are addressed here by considering two geometries when modelling the MUST flow configuration with the upstream flow directed perpendicular to the front array of the containers: a first geometry has the containers of identical size and perfectly aligned within the array, and a second realistic geometry includes the small irregularities present in the MUST field experiment. The wind-tunnel experimental data of Bezpalcova (2007) are used as a reference for our comparative study.

The paper is organised as follows: In Sect 2, a brief description of the MUST experiment is given, and the computational settings are described in Sect. 3. The results are presented in Sect. 4 and ordered as follows: first a comparison between RANS, LES and wind-tunnel measurements based on a statistical analysis is given in Sect. 4.1; secondly, the comparisons based on the local mean flow velocity and Reynolds shear stress is carried out by analysing the small geometrical irregularity effects in Sect. 4.2; in Sect. 4.3, this comparative analysis is provided for the spatially-averaged flow properties. Finally some concluding remarks are given in Sect. 5.

A comparative study of RANS and LES approaches for the simulation of passive contaminant dispersion in the MUST field experiment configuration is presented in Part II (Dejoan et al. 2010).

2 Brief Description of the MUST Experiment

The MUST field experiment was conducted in September 2001 at the Horizontal Grid, U.S. Army Dugway Proving Ground (DPG) by the Defence Threat Reduction Agency (DTRA). Many research agencies and universities have collaborated in the development of this experiment: U.S. Army Atmospheric Research Laboratory, Canadian Defence Research Establishment Suffield (DRES), UK Defence Science and Technology Laboratory (DSTL), U.S. Department of Energy (DOE), Los Alamos National Laboratory (LANL), Arizona State University (ASU) and the University of Utah. The experiment was designed to study the dispersion of a tracer through a large array of obstacles, to overcome the scaling constraints and measurement limitations of laboratory experiments and to obtain datasets at a near realistic scale useful for urban dispersion modelling (Biltoft 2001). A 12×10 aligned array of shipping containers was used to simulate the urban environment. Each container was 12.2 m long, 2.42 m wide and 2.54 m height, except for the one identified as H5, which was 6.1 m long, 2.44 m wide and 3.51 m height. In addition, the configuration of the array is slightly irregular due to several alignment errors. The average obstacle spacing is $\langle L_x \rangle / h = 5.08$ in the lengthwise direction (x-direction) and $\langle L_y \rangle / h = 3.11$ in the span-wise direction (y-direction), where h is the height of the standard container. A plan view of the irregular array is shown in Fig. 1. The array forms an angle of 30° to the north. The experimental set-up is described in detail in Biltoft (2001) and Yee and Biltoft (2004). Similar measurements with the same configuration (including the geometrical irregularities) were performed in the wind tunnel of the University of Hamburg within a scaled model (1:75) by Bezpalcova (2007); the flow properties were recorded using laser Doppler anemometry (Leitl et al. 2007). The Reynolds numbers, $Re = U_{\text{inlet}} h / \nu$, based on the inlet velocity, U_{inlet}, the height of the container, h, and the kinematic viscosity, ν, are approximately 10^6 in the field experiments and 10^4 in the wind-tunnel experiments.

The experimental data used in the comparative analysis presented here belong to one trial of the wind-tunnel experiment of Bezpalcova (2007) and Leitl et al. (2007) for which the

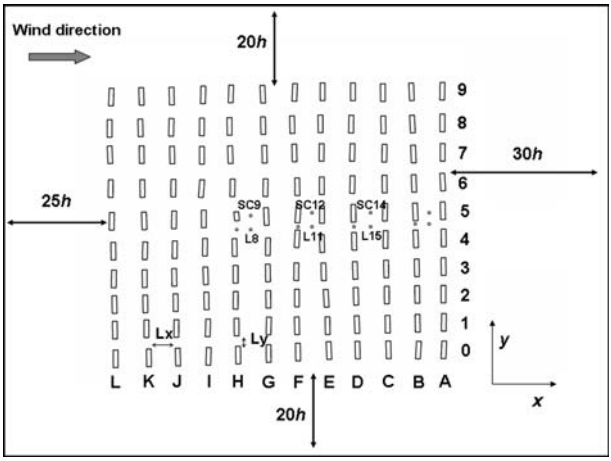

Fig. 1 Irregular array geometry: plan view of the real MUST geometry

inlet flow conditions are well controlled. Here, we make use only of the wind-tunnel measurements corresponding to the case with an upstream flow impinging perpendicularly to the array of the containers. Part II (Dejoan et al. 2010) will focus upon data from the field experiment with a different wind direction.

3 Computational Procedure

3.1 Flow Equations and Numerical Methods

In both the LES and RANS calculations a neutral turbulent flow was considered, i.e., without including buoyancy and stratification effects. In the LES approach, the large-scale flow is described by the filtered incompressible Navier–Stokes equations,

$$\frac{\partial \widetilde{U}_i}{\partial t} + \frac{\partial \widetilde{U_j U_i}}{\partial x_j} = -\frac{\partial \widetilde{P}}{\partial x_i} + \nu \frac{\partial^2 \widetilde{U}_i}{\partial x_j \partial x_j} - \frac{\partial \tau_{ij}}{\partial x_j} \tag{1}$$

where $\widetilde{U}_i$, $\widetilde{P}$ define the filtered velocity component and the filtered pressure, respectively, and ν is the fluid kinematic viscosity. The contribution of the subgrid scale to the resolved flow variables, represented by the stress tensor τ_{ij}, is modelled by the standard Smagorinsky model (Smagorinsky 1963)

$$\tau_{ij} = -2\nu_{sgs}\widetilde{S}_{ij} = (C_s \Delta)^2 \left|\widetilde{S}\right| \widetilde{S}_{ij} \tag{2}$$

where $\widetilde{S}_{ij} = 0.5(\partial \widetilde{U}_i/\partial x_j + \partial \widetilde{U}_j/\partial x_i)$ is the filtered strain tensor and ν_{sgs} is the subgrid-scale viscosity. The Smagorinsky constant C_s is set to a value of 0.1 and the filter width, Δ, is deduced from the grid computational size. Due to its simplicity and low computational cost, the Smagorinsky subgrid-scale model is at the moment the most commonly used in LES flow for urban-like geometry (Xie and Castro 2006, 2009).

The LES simulations were performed using as a baseline code the open source CFD code OpenFoam (2006). The numerical method incorporated in this package to discretize Eqs.

1 and 2 is based on the finite volume method formulated in a collocated grid arrangement. A Pressure Implicit Splitting of Operators (PISO) algorithm with two corrector steps is used to couple the velocity and the pressure. An incomplete-Cholesky preconditioned bi-conjugate gradient algorithm is used to solve the linearised equations of the velocity components while an algebraic multi-grid solver is used for the discretised pressure Poisson equation. A Rhie–Chow interpolation is used for the pressure gradient terms to avoid pressure oscillations due to the collocated grid arrangement. The temporal integration is performed by using the second-order semi-implicit backward scheme and the spatial derivatives are discretised according to the second-order central differencing scheme.

The RANS calculations were carried out by making use of FLUENT code (Fluent Inc. 2005) to solve the steady incompressible RANS equations; the turbulence closure used is the standard k–ε model. The governing equations are:

$$\overline{U}_j \frac{\partial \overline{U}_i}{\partial x_j} = -\frac{1}{\rho}\frac{\partial \overline{P}}{\partial x_i} + \frac{\mu}{\rho}\frac{\partial^2 \overline{U}_i}{\partial x_j \partial x_j} - \frac{\partial}{\partial x_j}(\overline{u_i' u_j'}), \tag{3}$$

$$\overline{U}_j \frac{\partial k}{\partial x_j} = \frac{1}{\rho}\frac{\partial}{\partial x_j}\left[\left(\mu + \frac{\mu_t}{\sigma_k}\right)\frac{\partial k}{\partial x_j}\right] + \frac{G_k}{\rho} - \varepsilon, \tag{4}$$

$$\overline{U}_j \frac{\partial \varepsilon}{\partial x_j} = \frac{1}{\rho}\frac{\partial}{\partial x_j}\left[\left(\mu + \frac{\mu_t}{\sigma_\varepsilon}\right)\frac{\partial \varepsilon}{\partial x_j}\right] + \frac{1}{\rho}C_{\varepsilon 1} G_k \frac{\varepsilon}{k} - C_{\varepsilon 2}\frac{\varepsilon^2}{k}, \tag{5}$$

where k is the turbulent kinetic energy and ε is the dissipation rate of turbulent kinetic energy, μ is the dynamic viscosity, $-\overline{u_i' u_j'} = \frac{1}{\rho}\mu_t\left(\frac{\partial \overline{U}_i}{\partial x_j} + \frac{\partial \overline{U}_j}{\partial x_i}\right) - \frac{2}{3}k\delta_{ij}$ is the Reynolds stress, μ_t is the turbulent viscosity expressed as $\mu_t = \rho C_\mu \frac{k^2}{\varepsilon}$, G_k is the turbulent kinetic energy production, σ_k ($= 1.0$) and σ_ε ($= 1.3$) are the turbulent Prandtl numbers for k and ε, respectively, the model constants C_μ, $C_{\varepsilon 1}$ and $C_{\varepsilon 2}$ take the respective standard values 0.09, 1.44 and 1.92 that were used for a wide range of turbulent flows (Launder and Spalding 1974; Versteeg and Malalasekera 1995). Note that in LES the Reynolds shear stress is a direct output of the simulation while in RANS it is fully modelled (see above relation).

The RANS governing equations are solved in a collocated grid system using a finite volume method. The pressure–velocity coupling is solved by means of the semi-implicit method for pressure-linked equations algorithm (SIMPLE) (Patankar 1980). A second-order upwind scheme is used for the discretisation of the advection terms.

3.2 Computational Set-Up

3.2.1 Flow Geometries and Parameters

In our simulations, two geometry configurations were taken into account: the first geometry is composed of an array of containers all having identical size and shape and perfectly aligned. The second geometry considered includes the irregularities of the MUST experiment configuration. Note that in the wind-tunnel experiment the MUST scaled model also contains the geometrical irregularities. These two flow configurations will be referred to as "the regular array case" and "the irregular array case", respectively. An overview of these geometries is given in Figs. 1 and 2.

In the regular array case, the computational domain was limited to a few rows of containers of the MUST geometry. As shown in Figs. 2a and b, the RANS regular array was composed of five rows of twelve containers while the LES domain includes three rows of eight containers.

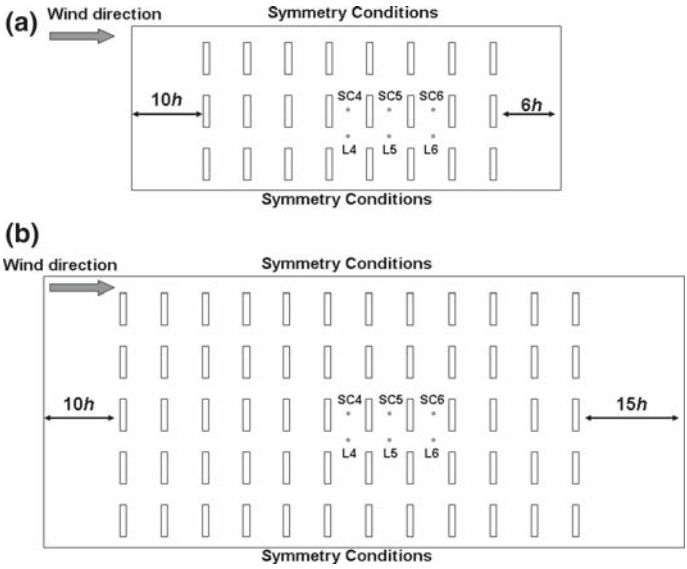

Fig. 2 Regular array geometry: plan view of the simplified MUST configuration, **a** LES and **b** RANS

At the lateral boundaries of the domain, symmetry conditions were applied, which is equivalent to simulating an infinite array of containers in the span-wise direction. This reduced computational domain allows us to perform calculations with a relative fine resolution at reasonable computing costs (in particular for LES) and can be justified by the experimental study of Meinders and Hanjalic (1999) who observed that flow patterns repeat along the streamwise and span-wise directions inside a regular array of obstacles. Note that, the regular array of containers presents the same average geometry characteristics as the field experiment geometry. In the irregular case, the computational domain covers the full MUST array (12×10 containers) and includes the small non-alignment and small variations in size and shape of the containers (see Fig. 1).

The upper limit of the domain is located both for LES and RANS at $11h$ in the regular case and at $8h$ in the irregular case. The extensions of the domain in the streamwise and lateral directions are given for each geometry in Figs. 1 and 2.

The Reynolds number, based on the inlet velocity, U_{inlet}, the height of the container, h, and the kinematic viscosity, ν, is set to $Re = U_{\text{inlet}}h/\nu = 4{,}700$ in the regular array case and to $Re = 10^6$ in the irregular array one. Note that, for the irregular geometry, the Reynolds number used is the same as that in the field experiment while in the regular geometry the Reynolds number is approximately half that in the wind-tunnel experiment. Both Reynolds numbers satisfy the criterion ($Re > 4{,}000$) given by Snyder (1981) and by Castro and Robins (1997) for Reynolds-number independency in the physical modelling of flows around obstacles. A more recent experimental study on the Reynolds-number-independency assumption by Lim et al. (2007) showed that, in certain circumstances (mainly related to the presence of strong vortex motion), flow quantities can be Reynolds-number dependent. However, in the present case, where the incident flow is oriented perpendicularly to the front of the obstacles, the Reynolds-number dependency is expected to be small on the mean and fluctuating velocity fields, in agreement with the results obtained by Lim et al. (2007) for the flow over a cube with an incident flow normal to the front face of the cube (a significant

Reynolds-number dependency was only found on the fluctuating surface pressure field for this configuration).

3.2.2 Grid Resolution

Preliminary grid resolution tests were performed for flow over a single container at the Reynolds number, $Re = 10^6$. Periodic boundary conditions were applied at the streamwise and lateral edges of the single container computational domain and a free-slip condition at the top. In the periodic streamwise direction the mean flow motion was induced by applying a constant streamwise mean pressure gradient in the RANS simulations and a constant flow rate in the LES. In the RANS calculations four grid tests (grids 0–3) were considered while in LES three grid tests (grids 1–3) were analyzed as given in Table 1. The influence of grid resolution for the single container configuration is shown in Fig. 3 for the profiles of the mean Reynolds shear stress at two locations about the container that corresponds to the positions SC and L indicated on Fig. 1. RANS calculations show that the shear-stress profile presents small differences between grids 1 and 2, and it is almost identical between grids 2 and 3. Grid systems 2 and 3 correspond to an increase in the number of grid cells for the discretization of the single container by a factor 8 (doubling the number of cells of grid 1 in each direction) and 64 (quadrupling the number of cells of grid 1 in each direction), respectively. At location SC the shear-stress profiles almost collapse while at location L some grid dependency is observed. Nevertheless, at this location the shear stress is low and the grid effects are not significant. Regarding the LES, the shear-stress profile varies a little from grids 1 to 3, especially at location SC where all profiles are very similar. At location L, the shear stress is identical in grids 1 and 2 but shows a higher peak in grid 3. Note that RANS shear-stress profiles exhibit a different shape than LES and that the peak value of the shear stress is higher in RANS than in LES. Beside the difference in the modelling approach, this may be in part explained by the different driving force methods used to maintain the mean flow in the periodic streamwise direction (in RANS a constant mean streamwise pressure gradient is used, while in LES the mean flow is sustained by forcing directly the mean flow rate to be constant). The RANS and LES velocity profiles showed a similar grid-resolution influence as for the respective shear stress (not shown here). For the RANS simulations, only grid 0 (coarsest grid) gives strong differences in the streamwise velocity predictions. Since the differences observed in the flow quantities, when comparing grids 1 and 2, are small and for the sake of keeping reasonable computing time (in particular for the LES) the number of grid points across the buildings used for the simulations of the full irregular case domain was kept as in grid 1 ($11 \times 4 \times 10$) for both RANS and LES simulations. In the regular case the computational domain is smaller than in the irregular case, which allowed for more savings regarding computing time and to make use of a little more refined grid resolution than grid 1 in RANS ($15 \times 5 \times 10$) and LES ($16 \times 5 \times 12$). The grids used in the present LES are between the requirements given by Tseng et al. (2006) (6 grid points per edge) and Xie and Castro (2006) (20 grid points per edge) to reasonably resolve the flow over cuboid-shape obstacles with LES. Note that making use of grid 3 in LES would lead to a quite extensive usage of computing time, a factor of about 20 approximately compared to grid 1. We recall here that our purpose is to make use of LES to resolve reasonably well the large scales dictated by the building sizes while keeping an affordable computational cost as compared to the RANS requirements. The energy spectra obtained using LES, given in Fig. 4 for the irregular and regular geometry cases at two locations behind the containers, exhibit a limited inertial range but show that the smallest resolved flow turbulence scales are well located in the inertial subrange.

Table 1 Grid characteristics

	Regular		Irregular		Grid test 0		Grid test 1		Grid test 2		Grid test 3	
	LES	RANS	LES	RANS	LES	RANS	LES	RANS	LES	RANS	LES	RANS
Total cells	$\approx 1.1 \times 10^6$	$\approx 1.3 \times 10^6$	$\approx 1.6 \times 10^6$	$\approx 1.6 \times 10^6$	–	$\approx 1.4 \times 10^3$	$\approx 1.7 \times 10^4$	$\approx 1.3 \times 10^4$	$\approx 1 \times 10^5$	$\approx 1 \times 10^5$	$\approx 3.7 \times 10^5$	$\approx 7 \times 10^5$
Gridpoints containers length	16	15	11	11	–	6	11	11	24	22	34	44
Gridpoints containers width	5	5	4	4	–	2	4	4	8	8	12	16
Gridpoints containers height	12	10	10	10	–	5	10	10	16	20	22	40

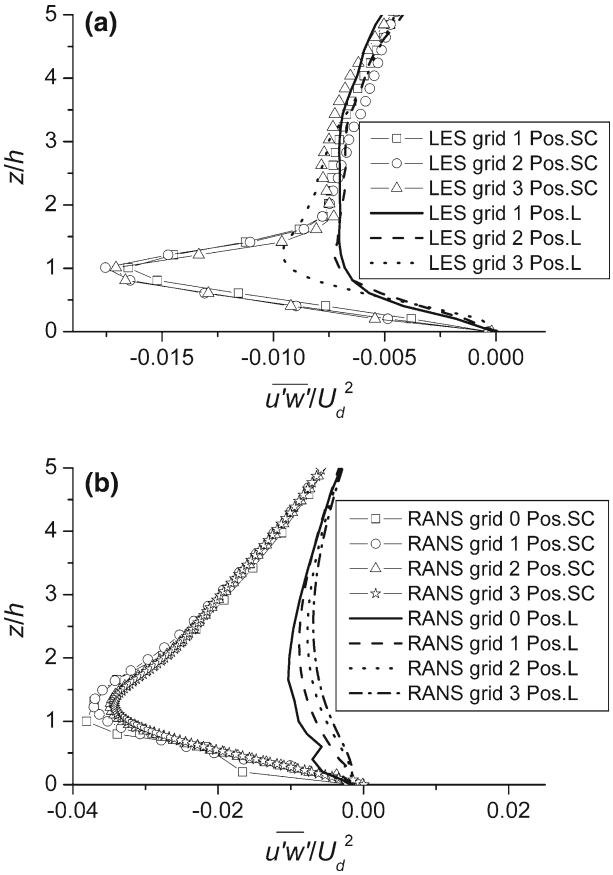

Fig. 3 Grid resolution tests over one single unit container: vertical profiles of the mean Reynolds shear stress: **a** LES simulations and **b** RANS simulations. The normalization used is by reference to the flow rate velocity, U_d. The locations SC and L are equivalent to the locations SC1–SC4 and L1–L4 around the container (see Figs. 1 and 2)

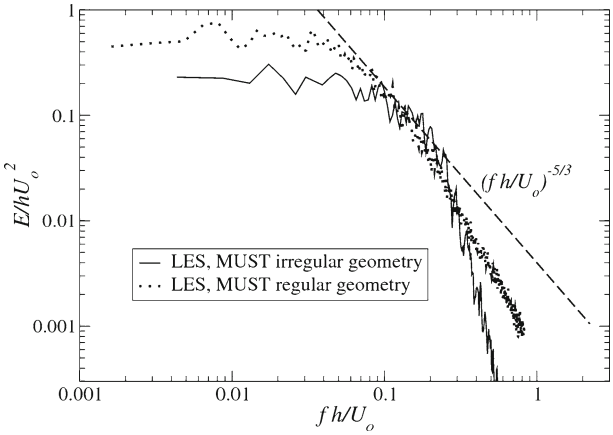

Fig. 4 Energy spectra obtained from the LES simulations of the regular and irregular cases

3.2.3 Boundary Conditions

The inflow condition applied in the RANS calculations of the regular array case is extracted from a preliminary RANS simulation of a fully turbulent flow in a periodic channel whose cross-section is identical to the one that contains the obstacles. The inflow velocity in the irregular case is fitted from the wind-tunnel experiment data of Bezpalcova (2007). In both regular and irregular cases, the boundary conditions applied at the walls consist of a standard logarithmic type boundary condition for the tangential stresses and a zero velocity orthogonal to the walls. At the top of the domains a free-slip condition is applied and at the outlet the pressure is prescribed and the velocity extrapolated from a zero-gradient condition.

In the LES, the wall, top and outflow boundary conditions are similar to those used in RANS. More recent approaches for LES wall boundary conditions in high Reynolds-number flows have been developed, such as wall modelling based on turbulent boundary-layer equations or hybrid RANS/LES (see Cabot and Moin 1999; Nikitin et al. 2000; Piomelli and Ballaras 2002). However, the use of a logarithmic-based wall boundary condition is the most commonly used in LES for flows over buildings (Tseng et al. 2006; Xie and Castro 2006, 2009). The use of the logarithmic-type wall boundary condition is based on the fact that viscous effects are negligible in such flows, the generation of turbulence being mainly associated with the large flow scales produced by the presence of the obstacles. For the inflow conditions, a mean velocity profile to which is added random noise is used. In the regular case a uniform velocity profile was used while in the irregular case the mean profile is fitted to the experimental wind-tunnel inflow data. Though not shown here, it was observed in the irregular case that the shape of the mean inlet profile (i.e. uniform or with a boundary layer fitted with the experimental data) has little influence on the flow quantities within the array that are presented here. The LES inflow condition used here is as simple as that used by Hanna et al. (2002) for flow within cubical obstacle arrays or by Smorlakiewicz et al. (2007) for flow over the Pentagon building, in the sense that the time and space correlations are not based on a physical content but on a random process. Only very recently, Xie and Castro (2009) developed an inflow approach for LES of street-scale flows. This approach was not considered here.

3.2.4 Integration Time in LES Simulations

The time step used in the LES is such that the Courant number does not exceed 0.6. The velocity statistics were accumulated over several "through flow" time units, $T = L_x/U_o$, after having reached a satisfactory developed turbulent field. For the regular geometry case the statistics were performed over a total time of $40T$, while in the case of the irregular geometry a total statistical time of $15T$ was used.

4 Results

A comparison between LES, RANS and experimental data is presented for the velocity and turbulence fields in the case of flow approaching the array perpendicular to the obstacles (see Fig. 1). The experimental data used for validation are those obtained from the wind-tunnel experiment of Bezpalcova (2007) and Leitl et al. (2007), which are the most complete datasets available for the flow quantities. The present comparison aims to gain insight into the effects of introducing geometrical irregularities, and how far their inclusion is relevant for the computation of such flows.

First, the RANS and LES results are compared with experimental data according to a statistical analysis for the irregular case only (wind-tunnel data correspond to the irregular case). Secondly, the results obtained with RANS and LES for the profiles of the mean velocity and turbulence field quantities are compared with measurements at several locations and are analysed for the regular and irregular cases. Then, information on the flow structure is given by considering the streamlines of the mean flow velocity. Finally, the results obtained for the horizontal spatially-averaged properties of flow quantities are compared in the regular and irregular cases.

All flow quantities are normalized by reference to the height of the obstacles, h, and the streamwise inlet velocity (U_o) taken at the height $z \approx 3h$.

4.1 Statistical Analysis

We use the wind-tunnel measurements of $\overline{U}$, $\overline{W}$ and $\overline{u'w'}$ for several vertical profiles (12 profiles, 317 data points) distributed inside the irregular array close to the H5, F5, D5 and B5 containers (Bezpalcova 2007; Leitl et al. 2007); the locations are indicated in Fig. 1. The experimental data cover a distance from the ground up to $5h$ approximately. The metrics used are the normalised square mean error (NMSE), fractional bias (FB), correlation coefficient (R), factor 2 (FAC2) and hit rate (q), defined as:

$$\text{NMSE} = \frac{\sum_{i=1}^{n} (O_i - P_i)^2}{\sum_{i=1}^{n} O_i \cdot \sum_{i=1}^{n} P_i}, \tag{6}$$

$$FB = \frac{\sum_{i=1}^{n} O_i - \sum_{i=1}^{n} P_i}{0.5 \cdot \left(\sum_{i=1}^{n} O_i + \sum_{i=1}^{n} P_i\right)}, \tag{7}$$

$$R = \frac{\sum_{i=1}^{n} \left[\left(O_i - \frac{1}{n}\sum_{i=1}^{n} O_i\right)\left(P_i - \frac{1}{n}\sum_{i=1}^{n} P_i\right)\right]}{\left[\sum_{i=1}^{n} \left(O_i - \frac{1}{n}\sum_{i=1}^{n} O_i\right)^2\right]^{1/2} \left[\sum_{i=1}^{n} \left(P_i - \frac{1}{n}\sum_{i=1}^{n} P_i\right)^2\right]^{1/2}}, \tag{8}$$

$$\text{FAC2} = \text{fraction of data that satisfy } 0.5 \leq P_i/O_i \leq 2.0, \tag{9}$$

$$q = \frac{1}{n}\sum_{i=1}^{n} N_i \text{ with } N_i = \begin{cases} 1 \text{ if } |(O_i - P_i)/O_i| \leq RD \text{ or } |O_i - P_i| \leq AD \\ 0 \text{ otherwise} \end{cases} \tag{10}$$

where n is the total number of sample points, O_i are the measured data and P_i are the predicted values, RD and AD represent the allowed relative deviation and the allowed absolute deviation of model results from the reference data, respectively. A relative deviation of $RD = 0.25$ for all variables and an absolute deviation of $AD = 0.05$ for normalised velocities ($\overline{U}/U_0$, $\overline{W}/U_0$) and $AD = 0.005$ for $\overline{u'w'}/U_0^2$ are used. The value of AD for normalised velocities and RD are similar to those used by Santiago et al. (2007) and Eichhorn (2004). Two analyses are made: one with the full dataset (Table 2) and the other with data corresponding to $z/h < 1$, i.e., within the canopy (110 data points, Table 3).

4.1.1 Hit Rate

The value of the hit rate for a successful validation based on the VDI guidelines (VDI 2005) is $q > 66\%$. For the full dataset, all variables fulfil this q limit. However, for the dataset within the canopy ($z/h < 1$) the hit rate decreases, indicating that in this zone the models have greater difficulties simulating the flow patterns accurately. Similar findings were found for RANS by Franke et al. (2008) who showed that RANS models for the MUST configuration

Table 2 Metrics computed from RANS and LES results for the irregular case with the full experimental dataset

	Hit rate	Hit rate*	FAC2	FB	NMSE	R
$\overline{U}/U_0$ (RANS)	0.77	0.74	0.896	0.031	0.03	0.949
$\overline{U}/U_0$ (LES)	0.76	0.75	0.849	0.108	0.04	0.960
$\overline{W}/U_0$ (RANS)	0.81	0.24	0.204	1.500	75.64	0.901
$\overline{W}/U_0$ (LES)	0.83	0.25	0.449	116	−10.34	0.866
$\overline{u'w'}/U_0^2$ (RANS)	0.67	–	0.902	0.180	0.26	0.639
$\overline{u'w'}/U_0^2$ (LES)	0.81	–	0.826	0.264	0.26	0.703

Hit rate* is the hit rate corresponding to more restricted values of AD ($AD = 0.008$ and 0.007 for $\overline{U}/U_0$, $\overline{W}/U_0$)

Table 3 Metrics computed from RANS and LES results for the irregular case with the experimental dataset inside the canopy

	Hit rate	Hit rate*	FAC2	FB	NMSE	R
$\overline{U}/U_0$ (RANS)	0.60	0.54	0.718	0.092	0.10	0.918
$\overline{U}/U_0$ (LES)	0.56	0.55	0.627	0.303	0.17	0.932
$\overline{W}/U_0$ (RANS)	0.70	0.15	0.074	1.111	22.65	0.892
$\overline{W}/U_0$ (LES)	0.71	0.25	0.370	15.379	−8.55	0.865
$\overline{u'w'}/U_0^2$ (RANS)	0.57	–	0.782	0.394	0.37	0.716
$\overline{u'w'}/U_0^2$ (LES)	0.53	–	0.645	0.494	0.51	0.676

Hit rate* is the hit rate corresponding to more restricted values of AD ($AD = 0.008$ and 0.007 for $\overline{U}/U_0$, $\overline{W}/U_0$)

give values of q under the limit for some flow quantities in some of the cases simulated. The hit rate q is strongly dependent on the values chosen for AD and RD. By making use of more restricted values of AD for normalised velocities, such as those used by Franke et al. (2008) ($AD = 0.008$ and 0.007 for $\overline{U}/U_0$, $\overline{W}/U_0$), the tendency of q to decrease is higher for the vertical velocity than for the streamwise velocity, see Tables 2 and 3. This behaviour is related to the very low values of $\overline{W}/U_0$ at the considered location where it is difficult to fulfil the RD criterion so that a change in AD affects strongly the value of q. The dependency of q upon AD is smaller for $\overline{U}/U_0$ because, in general, the values of $\overline{U}/U_0$ are high and it is easier to fulfil the RD criterion (most of them fulfil this criterion independently of the AD value). The difficulty of setting a meaningful value of q makes it worthwhile to consider other metrics to complete the statistical analysis.

4.1.2 Other Metrics

The values of FB, FAC2 and NMSE defined earlier are given in Tables 2 and 3. Similar to the hit rate, these values show a better fit with the experiments for the full dataset than for the data within the canopy. The positive values of FB indicate an underestimation of all flow variables by both models. In general, RANS and LES simulations have good correlation, with R close to 1 for the velocity components and around 0.7 for the Reynolds stress. The FAC2

and NMSE indicate a good agreement between the model results and the experimental data for the streamwise velocity and Reynolds stress but not for the vertical velocity. As for the hit rate q, the small values around zero (positive and negative) of $\overline{W}/U_0$ at the measurement locations means that in some cases the value of the statistical parameters is not meaningful.

Globally, LES and RANS computations give close values of hit rate and other metrics for both the streamwise velocity and Reynolds shear stress. These values indicate that both methodologies provide reasonable predictions. The vertical velocity is generally underestimated, even if LES performs better than RANS (better hit rate and FAC2).

The underestimation of $\overline{W}/U_0$ produced by RANS simulations is a known feature and was observed in a previous study by Olesen et al. (2008) and Franke et al. (2008) who compared the performance of various RANS models in the MUST flow configuration. A comparative analysis based on statistical metrics is helpful in estimating the errors in models, however it can lead to misleading conclusions since the experimental sample data are limited (i.e., only a few measurement locations). In the next section a comparison based on the mean flow profiles is given.

4.2 Mean Flow Field

4.2.1 Local Mean Velocity and Reynolds Stress Profiles

4.2.1.1 Regular Array Case. The profiles of the mean streamwise and vertical velocity components, $\overline{U}/U_0$ and $\overline{W}/U_0$, and of the Reynolds shear stress, $\overline{u'w'}/U_0^2$, obtained with RANS and LES computations are compared with experimental data in Fig. 5 at different locations inside the array. Note that the experimental data are extracted from the wind-tunnel experiment by Bezpalcova (2007) for the scaled model of the MUST field configuration that incorporates the geometrical irregularities. The locations selected for the comparisons are shown in Fig. 1 for the experiment and Fig. 2a and b for the simulations. The positions SC9, SC15, L9 and L14 are well located within the array so that the influence of inflow conditions can be minimized at these locations according to Meinders and Hanjalic (1999) who showed experimentally that far downstream of the inlet of a matrix of cubes the flow was developed and periodic. The simulations provide very similar profiles of the velocity components $\overline{U}/U_0$ and $\overline{W}/U_0$ at locations SC4–SC6. Along this line the RANS shear-stress profiles exhibit as well a very similar behaviour among the locations, while the LES shear-stress profiles exhibit a peak that tends to decrease going downstream of the array. Passing through positions L4–L6, the streamwise mean velocity component shows insignificant variations. However, if the mean vertical velocity component and the shear stress present similar profile shapes, some differences in the peak values are observed among the locations, and are more pronounced in the LES case. The velocity component $\overline{U}/U_0$ is closer to the measurements in the LES than in the RANS. For the mean vertical velocity component, $\overline{W}/U_0$, and the shear stress, $\overline{u'w'}/U_0^2$, the LES predicts higher values than RANS, the best agreement with the experiments being obtained with LES, in particular for $\overline{W}/U_0$ at the SC locations and $\overline{u'w'}/U_0^2$ at the L locations. A general tendency of RANS is to underestimate the vertical velocity and shear stress, in particular at L4–L6 where the values of $\overline{W}/U_0$ and $\overline{u'w'}/U_0^2$ are very low. Note that large discrepancies between both RANS and LES simulations and experiments are observed for $\overline{W}/U_0$ at the L locations. This is an effect of irregularities as will be shown in the next section.

4.2.1.2 Irregular array case. Figure 6 presents the comparisons of the mean velocity and Reynolds shear-stress profiles between the measurements and the results obtained by RANS

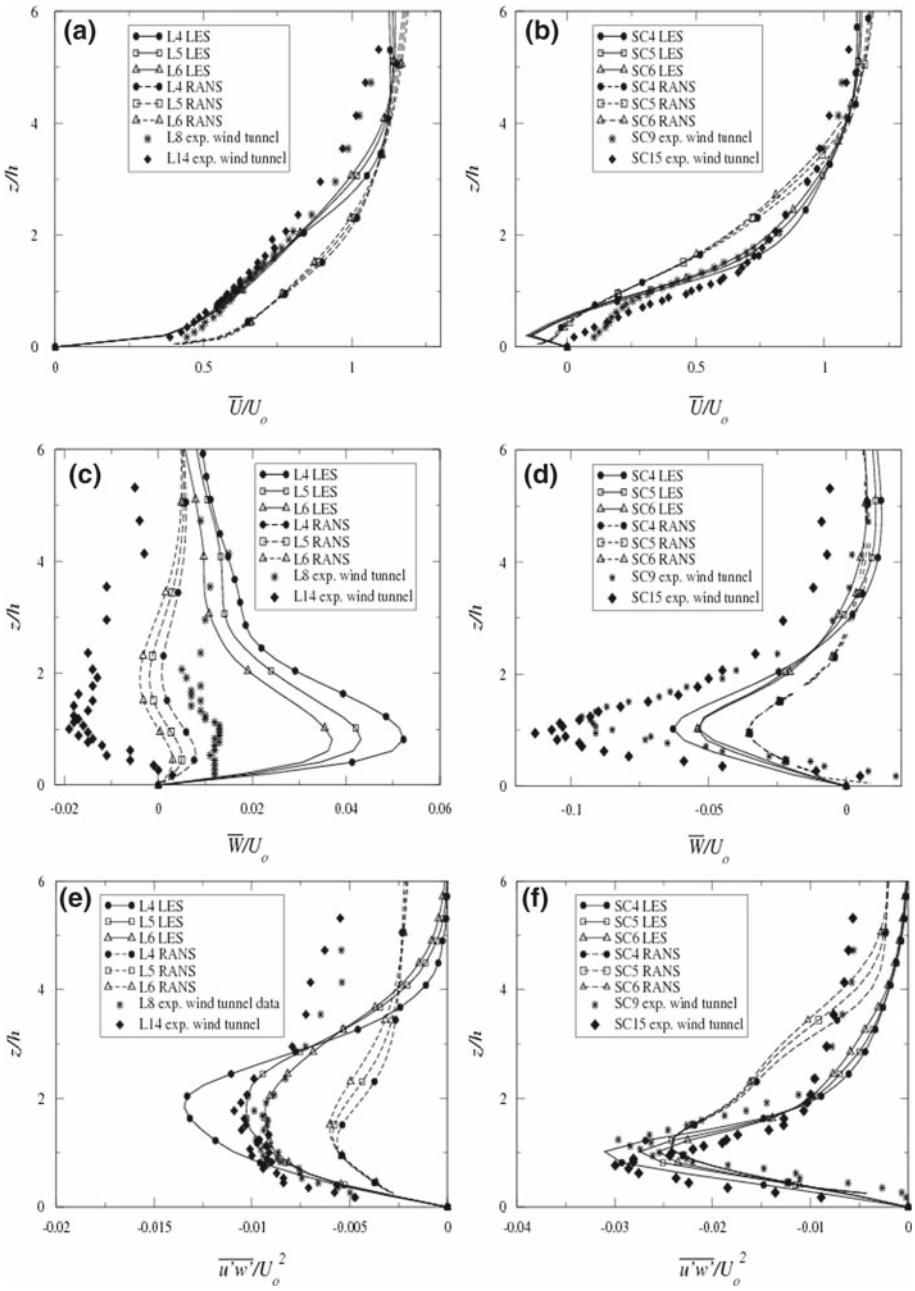

Fig. 5 Regular array simulations: **a** and **b** vertical profiles of the mean streamwise velocity, $\overline{U}/U_0$; **c** and **d** vertical profiles of the mean vertical velocity, $\overline{W}/U_0$; **e** and **f** vertical profiles of the Reynolds shear stress, $\overline{u_i' u_j'}/U_0^2$. Note that the wind-tunnel measurements were performed for the irregular array and that the locations are indicated in Figs. 1 and 2

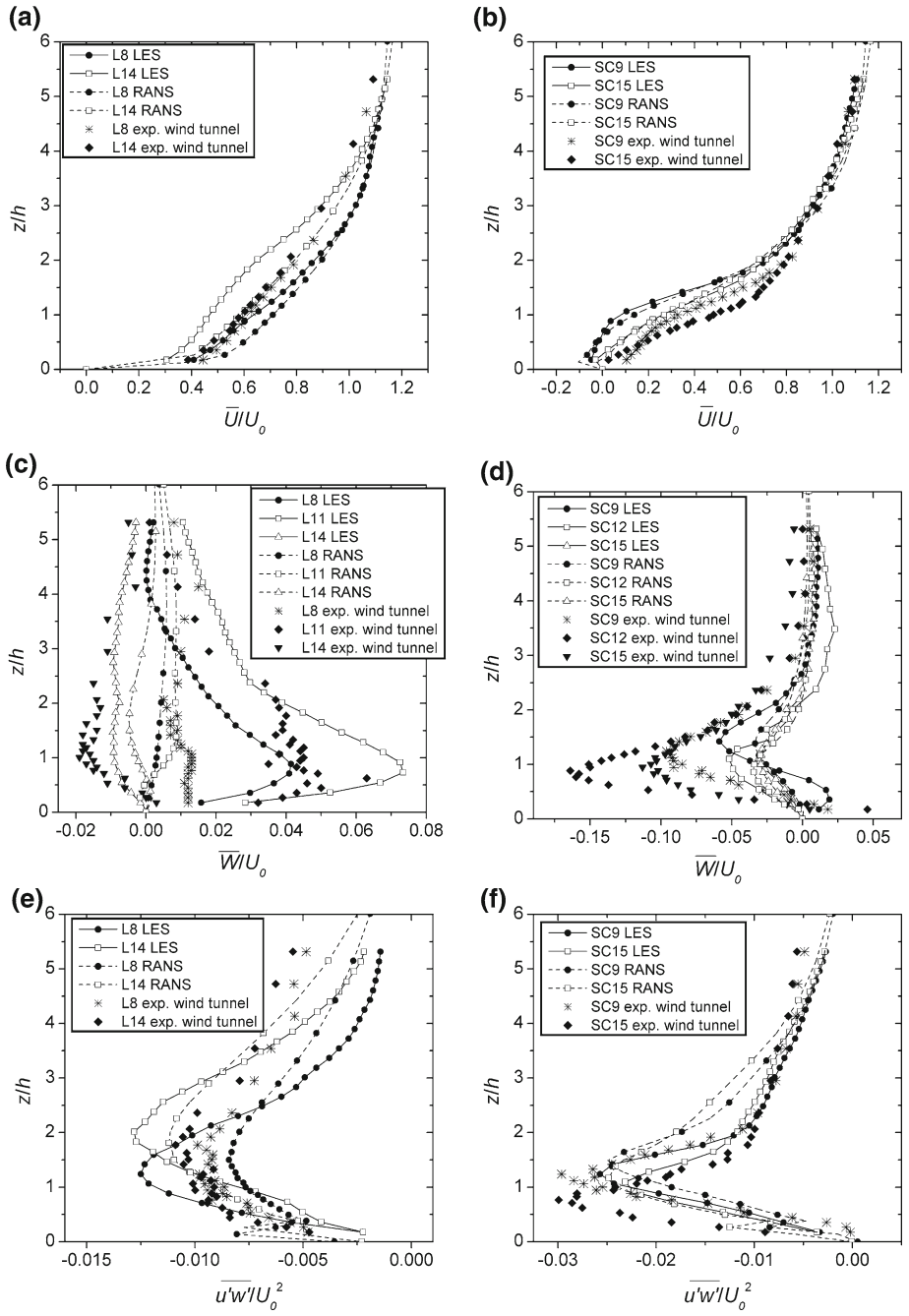

Fig. 6 Irregular array simulations: **a** and **b** vertical profiles of the mean streamwise velocity, $\overline{U}/U_0$; **c** and **d** vertical profiles of the mean vertical velocity, $\overline{W}/U_0$; **e** and **f** vertical profiles of the Reynolds shear stress, $\overline{u_i' u_j'}/U_0^2$ (see Fig. 1 for the locations)

and LES for the irregular array. The locations for the comparisons are shown in Fig. 1. The experimental data of $\overline{U}/U_0$ and $\overline{u'w'}/U_0^2$ show a small dependency on the locations SC9–SC15 and L9–L15, however $\overline{W}/U_0$ presents a strong variation along L9–L15 while it differs very little from SC9 to SC15. Regarding the simulations, at SC9–SC15 the irregularities have little effect on the RANS and LES streamwise mean velocity and on the shear-stress profiles, and are of the same order as those from the experiment. At locations L9–L15, the simulations show a somewhat higher influence from the irregularities than the experiments for $\overline{U}/U_0$. Figure 6c and d shows that LES captures better the variations of $\overline{W}/U_0$ than RANS, which provides values of the vertical velocity component that are too low. Regarding the other flow quantities, RANS and LES give similar results and, globally, a reasonable agreement is obtained with the measurements.

The comparison between the results obtained with RANS and LES for the regular and irregular cases and the experimental data (that include the geometrical irregularities) shows that the impact of the irregularity is the most significant for the vertical velocity component, especially along the L positions where the flow is channelled and the velocity profile changes in shape from one position to another. This behaviour is reasonably well predicted by LES but missed by RANS. Inside the recirculation flow regions the vertical velocity component is less affected by geometrical irregularities and the profile conserves a similar shape. The streamwise velocity component and shear-stress profiles are little affected by the irregularities whatever the locations considered and for these quantities LES and RANS give similar results that are in satisfactory agreement with experiments. Regarding the mean vertical velocity, LES provides a better prediction than RANS but both models show deficiencies in the overall predictions. As mentioned in the previous section, the underestimation of $\overline{W}/U_0$ is a common feature of RANS models (Olesen et al. 2008; Franke et al. 2008). Note that the mean vertical velocity takes small values at the considered locations, so that even if the relative error is high for this velocity component, the magnitude of the absolute error is probably comparable with that for the streamwise velocity.

4.2.2 Streamlines

Figures 7 and 8 show the averaged streamlines on a 2D plane for the mean flow velocity field obtained from LES and RANS simulations for the regular array. The x–z plane along the line defined by the SC locations (see Fig. 2) is considered in Fig. 7 and the plane x–y at altitude $z/h = 0.5$ in Fig. 8. When comparing LES and RANS it is observed that the recirculation zone behind the containers is larger in LES than in RANS. The smaller recirculation zone found in RANS is in agreement with the results of Sini et al. (1996). In addition, Castro and Apsley (1997) observed that the k–ε model poorly predicts the flow impingement and separation. Note that for RANS the flow re-attaches between two containers while this is not the case for LES.

The streamlines obtained from the simulations of the irregular array case in the x–y plane at altitude $z/h = 0.5$ are shown in Fig. 9, where it is seen that the inclusion of irregularities affects the flow locally. In particular the container of different shape and size located at $x/h \approx -8$ and $y/h \approx 4$ presents smaller downward recirculation zones, and the non-alignment of the containers in the region $2 < x/h < 10$ and $-10 < y/h < 10$ inhibits the formation of recirculation downstream of some of the containers. For this case both RANS and LES provide a similar behaviour. Again a tendency for RANS to predict smaller recirculation regions is observed. In general, the irregularities tend to break the repeated characteristic of the flow patterns observed in the regular geometry.

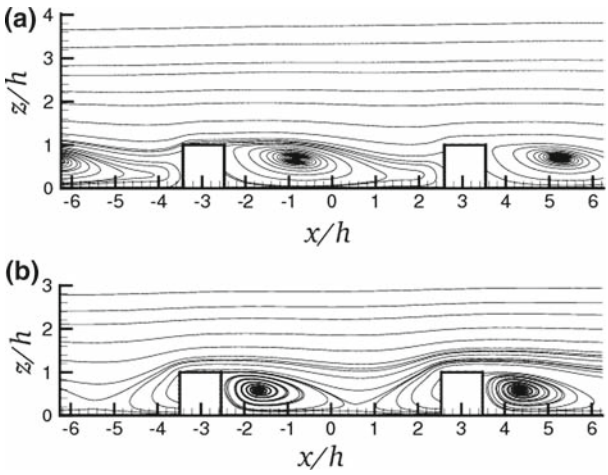

Fig. 7 Streamlines of the mean flow velocity field for the regular case in the plane (z–x) along the line described by SC locations (see Fig. 2). **a** LES; **b** RANS. Note that the 2D representation of the streamlines corresponds to the lines tangent to the velocity vector field projected in the corresponding plane

4.3 Spatially-Averaged Properties

As previously mentioned, in atmospheric (mesoscale) modelling of the urban environment, the whole city and its surrounding areas cannot be simulated (for computational reasons) at a resolution high enough to explicitly capture features of the flow around individual buildings. Therefore the urban canopy layer has to be parameterised to reproduce the effects of the complex morphology of a city (buildings, cars, gardens, etc) on the atmosphere. To determine the parameters required for atmospheric models, information is needed from spatial-averaged flow properties of the urban layer. Here, spatially-averaged properties of flow field quantities obtained from the LES and RANS simulations are compared.

The RANS model provides time-(or ensemble-) averaged values (indicated here by an overbar) and the extraction of spatially-averaged values (indicated by $\langle\ \rangle$) consists of averaging in space the time- (or ensemble-) averaged field variables. Regarding LES, the flow quantities are first averaged in time before applying the space average.

The spatial average of a variable ψ can be defined as (see Martilli and Santiago 2007),

$$\langle\overline{\psi}\rangle = \frac{1}{V_{\text{air}}}\int_{V_{\text{air}}} \psi(\vec{x},t)d\vec{x} \tag{11}$$

where $\langle\ \rangle$ denotes an horizontal space average operator. The spatial average of the streamwise and vertical velocity components, $\langle\overline{U}\rangle$ and $\langle\overline{W}\rangle$, of the Reynolds and dispersive shear stresses, $\langle\overline{u'w'}\rangle$ and $\langle\widehat{u}\,\widehat{w}\rangle$, are analysed as functions of vertical distance from the ground. The dispersive stress is related to the vortex formed in the street canyons (Martilli and Santiago 2007) and is defined as,

$$\widehat{u}\,\widehat{w}_{ij} = \left(\langle\overline{u}\rangle - \overline{u}_{ij}\right)\left(\langle\overline{w}\rangle - \overline{w}_{ij}\right), \tag{12}$$

Note that, usually, the dispersive stress is denoted as $\tilde{u}\tilde{w}$ but here is written as $\widehat{u}\,\widehat{w}$ to avoid confusion with the filtered LES variables represented with a tilde ($\sim$).

The spatially-averaged flow properties are given for the regular and irregular cases. In the regular array case, the horizontal average is applied over the central street canyon unit (one building and one canyon). In this way, the effects of the array borders on the flow are smoothed and the average properties made over this region are representative of the behaviour of the flow within the array. To also minimize border effects in the irregular array case,

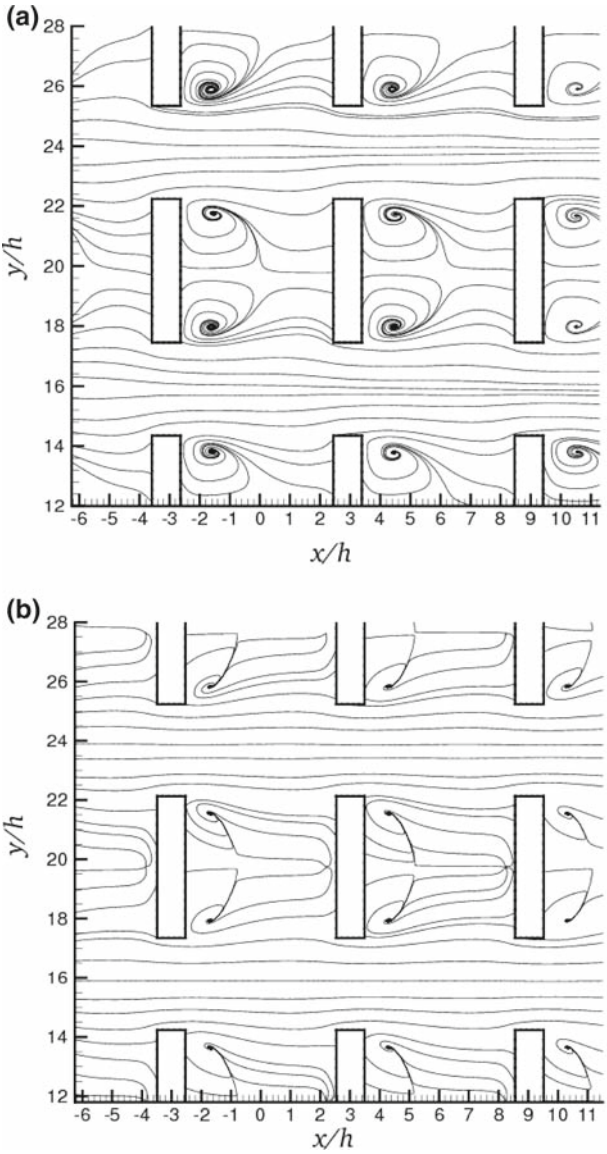

Fig. 8 Regular array simulations: streamlines of the mean flow velocity field in the plane (x–y) at $z/h = 0.5$. **a** LES; **b** RANS. Note that the 2D representation of the streamlines corresponds to the *lines* tangential to the velocity vector field projected in the corresponding plane

the spatial averages are performed over the whole array with the exception of the first row of building-canyon units around the array.

Figure 10 shows the profiles of the spatially-averaged variables $\langle \overline{U} \rangle / U_0$, $\langle \overline{W} \rangle / U_0$, $\langle \overline{u'w'} \rangle / U_0^2$ and $\langle \widehat{u}\,\widehat{w} \rangle / U_0^2$. Only slight differences are observed in the space average properties between RANS and LES for both the regular and irregular cases. The flow properties are also seen to be insignificantly modified by the presence of small irregularities. In particular,

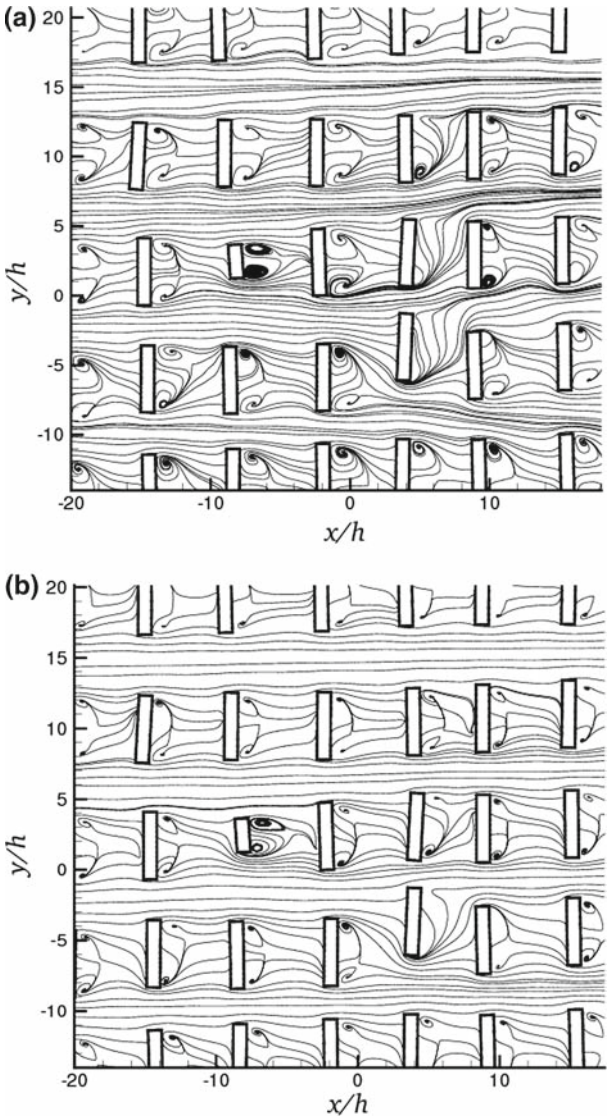

Fig. 9 Irregular array simulations: streamlines of the mean flow velocity field in the plane (x–y) at $z/h = 0.5$. **a** LES; **b** RANS. Note that the 2D representation of the streamlines corresponds to the *lines* tangential to the velocity vector field projected in the corresponding plane

the high spatial dependence observed on the time-averaged profile $\overline{W}/U_0$ (see Fig. 6c) is smoothed when the spatial average is applied. Regarding the dispersive stress, the RANS results are close to those for LES and both are found to be almost insensitive to small geometrical irregularities. The RANS and LES dispersive stresses are shown to be very small in comparison with the spatially-averaged shear stresses in the whole domain. Therefore, the dispersive stress can be neglected in comparison with the shear stress for this configuration from the point of view of urban canopy modelling. Note that the small values of the dispersive stress are related to the low packing density of this configuration. As commented above, the dispersive stress is associated with the vortex formed in the street canyons (Martilli and Santiago 2007). In the present case, the aspect ratio of these street canyons, defined as the

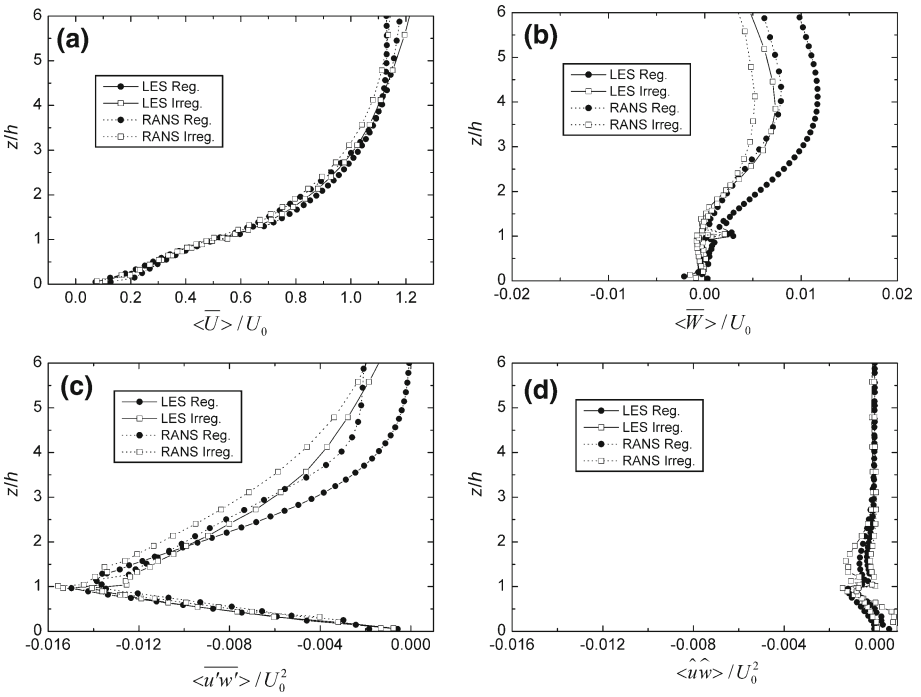

Fig. 10 Horizontal spatially-averaged flow properties: **a** vertical profiles of the mean streamwise velocity, $\langle\overline{U}\rangle/U_0$; **b** vertical profile of the mean vertical velocity, $\langle\overline{W}\rangle/U_0$; **c** vertical profiles of the Reynolds shear stress, $\langle\overline{u'w'}\rangle/U_0^2$; **d** vertical profiles of the dispersive stress, $\langle\widehat{u}\widehat{w}\rangle/U_0^2$

ratio of the width of the street and the height of the obstacle, is approximately 5 so that the flow regime is far from the skimming flow where the contribution of the dispersive fluxes can be important inside the urban canopy (Martilli and Santiago 2007).

The present RANS and LES results show that the spatially-averaged flow properties are not sensitive to small geometrical irregularities (as presented here). Moreover, the spatially-averaged flow properties of a reduced array, limited to one unit container, are shown to be very similar to the flow properties averaged over the full array of containers. This suggests that one part of a city can be represented by a simplified configuration (e.g., a periodic domain of one building-street unit) when spatial averages are of interest and that, for the reduced configurations, the CFD models can be helpful in improving canopy models by providing properties that are difficult to obtain experimentally (e.g., the assessment of drag coefficients).

5 Conclusions

In this study, RANS and LES are used to simulate the flow over the MUST field experiment geometry that is representative of a simplified urban environment. In the LES simulations presented here the grid mesh resolution was chosen in order to ensure a reasonable resolution of the large-scale flow generated by the containers while keeping the computing times two orders of magnitude below those needed for RANS calculations. The aim was to investigate the feasibility and the potential superiority of using LES compared to RANS for the simulation of flow within urban-like geometry at a relative low computational cost.

The comparative analysis used as a reference the wind-tunnel experimental data of Bezpalcova (2007) for a flow configuration with an upstream flow directed perpendicular to the front of the obstacles. The comparisons were based on a statistical analysis and by comparing mean flow quantities. For the mean flow quantities, effects of small geometrical irregularities were addressed at the microscale level (building flow scales) and at the mesoscale level (space-averaged flow properties).

A statistical analysis based on various metrics proposed in the literature showed a reasonably good prediction of the mean streamwise velocity and shear stress by LES and RANS; the mean vertical velocity is in general underpredicted by both methods, the LES providing however a better hit rate and FAC2 for this velocity component. This type of analysis is helpful in estimating the errors in models, but it can lead to misleading conclusions due to the limited number of experimental data available, and, as well, to the high dependence of some parameters used in the definition of the metrics for the error assessment. The differences observed in the flow structure between the RANS and LES are shown to not affect the similarity in the hit rate between the two computational approaches so that caution should be used when interpreting this metric.

At the microscale level, small irregularities are shown to affect significantly the mean vertical velocity component while the mean streamwise velocity and Reynolds shear stress are shown to be less sensitive to small geometrical perturbations. Their inclusion also breaks the repeated flow patterns found in an array of containers with identical shape and which are perfectly aligned. For the mean streamwise velocity and Reynolds shear stress, the present LES results are found to be close to RANS results and both approaches were in satisfactory agreement with the observations. However, LES captured better the irregularity effects observed on the vertical velocity components. The magnitude of this velocity component is in general underestimated by RANS.

At the mesoscale level, the small geometrical perturbation effects were found insignificant for both the spatially-averaged streamwise and vertical velocity components and as well for the spatially-averaged Reynolds shear stress. Regarding the dispersive stress, it was shown to be negligible compared to the spatially-averaged shear stress. Globally, the results obtained with LES and RANS for the spatially-averaged flow properties were found to be similar for each flow configuration considered and only slight differences were observed in the four cases studied (LES in regular and irregular arrays, and RANS in regular and irregular arrays). At this scale level, it was shown that the flow properties averaged over the full MUST array flow configuration are similar to the flow properties averaged over the one unit regular container flow configuration. This result is very relevant from the urban canopy modelling point of view because the spatially-averaged flow properties computed by CFD models in a simplified configuration can be representative of the average properties of a real part of a city without large irregularities, and can be used for the improvement of the parameterisation of atmospheric mesoscale models.

Acknowledgements The authors wish to thank J. M. White and B. Leitl for providing field data and wind-tunnel data from the MUST experiment, respectively and J. Franke for providing one of the meshes used in this study. The present study was funded by the Spanish Ministry of Defence.

References

Bezpalcova K (2007) Physical modelling of flow and dispersion in an urban canopy. PhD thesis, Faculty of Mathematics and Physics, Charles University, Prague, 193 pp

Biltoft CA (2001) Customer report for Mock Urban Setting Test (MUST). DPG document WDTC-TP-01-028, West Desert Test Center, U.S. Army Dugway Porving Ground, Dugway, Utah, 58 pp

Cabot W, Moin P (1999) Approximate wall boundary conditions in the large eddy simulation of high Reynolds number flow. Flow Turbul Combust 63:269–291
Camelli FE, Lohner R, Hanna SR (2005) VLES study of MUST experiment. In: 43rd AIAA Aerospace Meeting and Exhibit, January 10–13, Reno, Nevada, paper 1279, 19 pp
Castro IP, Apsley DD (1997) Flow and dispersion over topography: a comparison between numerical and laboratory data for two-dimensional flows. Atmos Environ 31:839–850
Castro IP, Robins AG (1997) The flow around a surface-mounted cube in uniform and turbulent streams. J Fluid Mech 79:307–335
Castro IP, Cheng H, Reynolds R (2006) Turbulence over urban-like roughness: deductions from wind-tunnel measurements. Boundary-Layer Meteorol 118:109–131
Cheng H, Castro IP (2002) Near wall flow over urban-like roughness. Boundary-Layer Meteorol 104:229–259
Cheng Y, Lien FS, Yee E, Sinclair R (2003) A comparison of large eddy simulations with a standard k–ε Reynolds-averaged Navier–Stokes model for the prediction of a fully developed turbulent flow over a matrix of cubes. J Wind Eng Ind Aerodyn 91:1301–1328
Coceal O, Belcher SE (2004) A canopy model of mean winds through urban areas. Q J Roy Meteorol Soc 130:1349–1372
Coceal O, Thomas TG, Castro IP, Belcher SE (2006) Mean flow and turbulence statistics over groups urban-like cubical obstacles. Boundary-Layer Meteorol 121:491–519
Dejoan A, Santiago JL, Martilli A, Martin F, Pinelli A (2010) Comparison between large-eddy simulation and Reynolds-averaged Navier–Stokes computations for the MUST field experiment. Part II: effects of incident wind angle deviation on the mean flow and plume dispersion. Boundary-Layer Meteorol. doi:10.1007/s10546-010-9467-2
Di Sabatino S, Buccolieri, Olesen H, Ketzel M, Berkowicz R, Franke J, Schatzmann M, Schlünzen H, Leitl B, Britter R, Borrego C, Costa AM, Trini-Castelli S, Reisin T, Hellsten A, Saloranta J, Moussiopulos N, Barmpas F, Brzozowski K, Goricsan I, Balczò M, Bartzis J, Efthimiou G, Santiago JL, Martilli A, Piringer M, Hirtl M, Baklanov A, Nuterman R, Starchenko A (2009) COST 732: in practice: the MUST model evaluation exercise. Int J Environ Pollut (in press)
Dobre A, Arnold SJ, Smalley RJ, Boddy JWD, Barlow JF, Tomlin AS, Belcher SE (2005) Flow field measurements in the proximity of an urban intersection in London, UK. Atmos Environ 39:4647–4657
Eichhorn J (2004) Application of a new evaluation guideline for microscale flow models. In: 9th international conference on harmonisation within atmospheric dispersion modelling for regulatory purposes, Garmisch-Partenkirchen, June 1–4, Germany, 5 pp
Flaherty JE, Stock D, Lamb B (2007) Computational fluid dynamic simulations of plume dispersion in urban Oklahoma City. J Appl Meteorol Clim 46:2110–2126
Fluent Inc. (2005) FLUENT 6.2 User's guide, vols 1–3. Fluent Inc., Lebanon, 2216 pp
Franke J, Bartzis J, Barmpas F, Berkowicz R, Brzozowski K, Buccolieri R, Carissimo B, Costa A, Di Sabatino S, Efthimiou G, Goricsan I, Hellsten A, Ketzel M, Leitl B, Nuterman R, Olesen H, Polreich E, Santiago JL, Tavares R (2008) The MUST model evaluation exercise: statistical analysis of modelling results. In: 12th international conference on harmonisation within atmospheric dispersion modelling for regulatory purposes, Cavtat, October 6–9, Croatia, 5 pp
Hanna SR, Tehranian S, Carissimo B, Macdonald RW, Lohner R (2002) Comparisons of model simulations with observations of mean flow and turbulence within simple obstacle arrays. Atmos Environ 36:5067–5079
Kastner-Klein P, Plate EJ (1999) Wind-tunnel study of concentration fields in street canyons. Atmos Environ 33:3973–3979
Kim JJ, Baik JJ (2004) A numerical study of effects of ambient wind direction on flow and dispersion in urban street canyons using the RNG k-ε turbulence model. Atmos Environ 38:3039–3048
Launder BE, Spalding DB (1974) The numerical computation of turbulent flow. Comput Method Appl Mech Eng 3:269–289
Leitl B, Bezpalcova K, Harms F (2007) Wind Tunnel Modelling Of The MUST Experiment. In: 11th international conference on harmonisation within atmospheric dispersion modelling for regulatory purposes, Cambridge, July 2–5, UK, 5 pp
Lim HC, Castro IP, Hoxey RP (2007) Bluff bodies in deep turbulent boundary layers: Reynolds-number issues. J Fluid Mech 571:97–118
Martilli A, Santiago JL (2007) CFD simulation of airflow over a regular array of cubes. Part II: analysis of spatial average properties. Boundary-Layer Meteorol 122:635–654
Martilli A, Clappier A, Rotach MW (2002) An urban surface exchange parameterization for mesoscale models. Boundary-Layer Meteorol 104:261–304
Meinders ER, Hanjalic K (1999) Vortex structures and heat transfer in turbulent flow over a wall-mounted matrix of cubes. Int J Heat Fluid Flow 20:255–267

Meroney RN, Pavegeau M, Rafailidis S, Schatzmann M (1996) Study of line source characteristics for 2D physical modelling of pollutant dispersion in street canyons. J Wind Eng Ind Aerodyn 62:37–56
Michioka M, Sato A (2009) Numerical simulations of gas dispersion in a residential area. In: The seventh international conference on urban climate, Yokohama, June 29-July 3, Japan, 4 pp
Milliez M, Carissimo B (2007) Numerical simulations of pollutant dispersion in an idealized urban area for different meteorological conditions. Boundary-Layer Meteorol 122:321–342
Nikitin NV, Nicoud F, Wasistho B, Squires KD, Spalart PR (2000) An approach to wall modelling in large eddy simulation. Phys Fluids 12:1629–1632
Olesen HR, Baklanov A, Bartzis J, Barmpas F, Berkowicz R, Brzozowski K, Buccolieri R, Carissimo B, Costa A, Di Sabatino S, Efthimiou G, Franke J, Goricsan I, Hellsten A, Ketzel M, Leitl B, Nuterman R, Polreich E, Santiago J, Tavares R (2008) The MUST model evaluation exercise: patterns in model performance. In: 12th international conference on harmonisation within atmospheric dispersion modelling for regulatory purposes, Cavtat, October 6–9, Croatia, 5 pp
OpenFoam (2006) Version 1.3, User and Programmer guide. Technical Report. http://www.opencfd.co.uk/openfoam
Patankar SV (1980) Numerical heat transfer and fluid flow. Hemisphere Publishing Corporation, New York, 197 pp
Pavageau M, Schatzmann M (1999) Wind tunnel measurements of concentration fluctuations in an urban street canyon. Atmos Environ 33:3961–3971
Piomelli U, Ballaras E (2002) Wall-layer models for Large Eddy Simulations. Annu Rev Fluid Mech 34:349–374
Santiago JL, Martilli A, Martin F (2007) CFD simulation of airflow over a regular array of cubes. Part I: three-dimensional simulation of the flow and validation with wind-tunnel measurements. Boundary-Layer Meteorol 122:609–634
Santiago JL, Coceal O, Martilli A, Belcher SE (2008) Variation of the sectional drag coefficient of a group of buildings with packing density. Boundary-Layer Meteorol 128:445–457
Sini JF, Anquetin S, Mestayer PG (1996) Pollutant dispersion and thermal effects in urban street canyons. Atmos Environ 30:2659–2677
Smagorinsky J (1963) General circulation experiments with the primitive equations. Mon Weather Rev 91(3):99–164
Smorlakiewicz PK, Sharman R, Weil J, Perry SGc, Heist D, Bowker G (2007) Building resolving large-eddy simulations and comparison with wind tunnel experiments. J Comput Phys 227:633–653
Snyder W (1981) Guidelines for fluid modelling of atmospheric dispersion. Report Number EPA-600/8-81-009, Environmental Protection Agency, Research Triangle Park, NC, 200 pp
Tseng Y-H, Meneveau C, Parlange M (2006) Modeling flow around bluff bodies and predicting urban dispersion using large eddy simulation. Environ Sci Technol 40:2653–2662
VDI (2005) Environmental meteorology—prognostic microscale windfield models—evaluation for flow around buildings and obstacles. VDI guidelines 3783, Part 9, Beuth, Berlin
Versteeg HK, Malalasekera W (1995) An introduction to computational fluid dynamics. The finite volume method. Person Prentice Hall, Harlow, 272 pp
Xie Z, Castro IP (2006) LES and RANS for turbulent flow over arrays of wall-mounted obstacles. Flow Turbul Combust 76:291–312
Xie Z, Castro IP (2009) Large-eddy simulation for flow and dispersion in urban streets. Atmos Environ 43:2174–2185
Yakhot A, Anor T, Liu H, Nikitin N (2006) Direct numerical simulation of turbulent flow around a wall-mounted cube: spatio-temporal evolution of large-scale vortices. J Fluid Mech 566:1–9
Yee E, Biltoft CA (2004) Concentration fluctuation measurements in a plume dispersing through a regular array of obstacles. Boundary-Layer Meteorol 111:363–415
Yee E, Gailis RM, Hill A, Hilderman T, Kiel D (2006) Comparison of wind tunnel and water-channel simulations of plume dispersion through a large array of obstacles with a scales field experiment. Boundary-Layer Meteorol 121:389–432